frontiers in Physics

ORIGINAL RESEARCH
published: 19 November 2020
doi: 10.3389/fphy.2020.567732

Estimating the Relative Biological Effectiveness of Auger Electron Emitter ^{123}I in Human Lymphocytes

Hein Fourie[1†], Shankari Nair[2†], Xanthene Miles[2], Daniel Rossouw[2], Philip Beukes[3], Richard T. Newman[1], Jan Rijn Zeevaart[4], Charlot Vandevoorde[2] and Jacobus Slabbert[2]*

[1]Department of Physics, Stellenbosch University, Stellenbosch, Cape Town, South Africa, [2]Nuclear Medicine Department, NRF iThemba LABS, Cape Town, South Africa, [3]Department of Radiation Safety Health Environment and Quality, iThemba LABS, Cape Town, South Africa, [4]Department of Radiochemistry, South African Nuclear Energy Corporation, Pretoria, South Africa

OPEN ACCESS

Edited by:
Yolanda Prezado, INSERM U1021 Signalisation normale et pathologique de l'embryon aux thérapies innovantes des cancers, France

Reviewed by:
Dimitris Emfietzoglou, University of Ioannina, Greece
Jean-Pierre Pouget, Institut National de la Santé et de la Recherche Médicale (INSERM), France

***Correspondence:**
Shankari Nair
snair@tlabs.ac.za

†These authors have contributed equally to this work.

Specialty section:
This article was submitted to Medical Physics and Imaging, a section of the journal Frontiers in Physics

Received: *30 May 2020*
Accepted: *14 October 2020*
Published: *19 November 2020*

Citation:
Fourie H, Nair S, Miles X, Rossouw D, Beukes P, Newman RT, Zeevaart JR, Vandevoorde C and Slabbert J (2020) Estimating the Relative Biological Effectiveness of Auger Electron Emitter ^{123}I in Human Lymphocytes. Front. Phys. 8:567732. doi: 10.3389/fphy.2020.567732

Auger electron emitters are considered to be a promising strategy for targeted radionuclide therapy of metastatic diseases, given their high linear energy transfer (LET) and short range in tissue which could potentially limit normal tissue toxicity. Particularly Auger electron emitters that can be targeted into the DNA of tumor cells have been considered as an attractive cancer therapy in the past decade. In this study, the efficiency of the Auger electron emitter ^{123}I (half-life 13.2 h) to induce chromosomal damage was investigated by using the cytokinesis-block micronucleus assay. A stannylated deoxyuridine was synthesized and radiolabeled with ^{123}I, resulting in ^{123}IUdR that carried the Auger electron emitter across the nuclear membrane and allowed its incorporation into newly synthesized DNA. The DNA damage caused by the ^{123}I Auger cascade was estimated by evaluating the induced micronuclei frequencies in human peripheral blood lymphocytes obtained from three different donors. The isolated lymphocytes were stimulated with phytohemagglutinin (1 mg/ml) for 48 h before pulse labeling with ^{123}IUdR and the S-phase fraction was determined using flow cytometry. Geant4 Monte Carlo calculations were performed to determine the absorbed dose in cells by the Auger emitter. The relative biological effectiveness (RBE) was calculated by comparing the dose response curves for ^{123}IUdR with the reference dose response curves, obtained with ^{60}Co γ-ray irradiation in this study, for lymphocytes of the same donors. This resulted in a range of individual RBE values from 3 up to 10, depending on the donor and the radiation dose. In addition, dose limiting RBE values (RBE_{Max}) were calculated for each donor and ranged from 5 to 11, dependent on the inherent radiosensitivity of the donors. This study provides valuable information on the RBE of Auger electron emitter ^{123}I, which is identified as a promising theranostic radionuclide for future targeted radionuclide therapy.

Keywords: iododeoxyuridine, auger electron, ^{123}I, micronucleus assay, relative biological effectiveness, GEANT4 Monte Carlo simulations

INTRODUCTION

The Auger effect refers to the emission of a cascade of low energy electrons, including Auger, Coster-Kronig (CK), and super-CK electrons (collectively called Auger electrons) as a result of radioactive decay by electron capture or internal conversion. Both processes result in the creation of inner shell electron vacancies that are filled by electron transitions from shells of higher energy, resulting in the release of energy either as characteristic x-rays or as low-energy Auger electrons [1, 2]. The Auger effect was first discovered in independent work by Lize Meitner and Pierre Auger in the 1920's [3–5]. Many radionuclides that are commonly used in nuclear medicine follow this decay process, including ^{123}I, ^{125}I, ^{67}Ga, ^{99}mTc, ^{111}In, ^{201}Tl and others as described in Ref. 6. However, it took many years since the discovery of Auger electrons before radiobiologists observed the extreme cytotoxic effect of Auger electron emitters, particularly when they are incorporated into the nucleus of cells [7, 8]. This prompted the interest to use Auger electron emitters as a promising radionuclide therapy for the treatment of various types of cancer [6, 9]. Radionuclide therapy, as an alternative to external beam radiotherapy or brachytherapy, almost exclusively uses energetic electrons from particle emitting isotopes. It takes advantage of their limited range in tissue in order to deliver relatively high doses to tumors whilst sparing surrounding healthy tissue. The most commonly used β-particle emitters have a tissue penetration range in the order of up to 1–10 mm, depending on the energy, characterized by a low linear energy transfer (LET) of approximately 0.2 keV/μm [10]. Consequently, high radionuclide concentrations are required in the targeted tissue to make them effective. The β-particle emitters also induce a cross-fire effect, which results in the irradiation of not only the target cell but additional neighboring cells in their range. This might be beneficial to homogenize the radiation dose in large solid tumors, but it is rather disadvantageous for the treatment of a small cluster of tumor cells and it might also result in greater hematological toxicity [10–12]. In recent years, α-particle emitters have regained interest and popularity, based on new, optimized production processes and the availability of various targeting vectors, such as monoclonal antibodies [13, 14]. Their range in tissues is about 50–100 μm depending on the α-particle energy. Since they deposit most of their energy at the end of their track in a very small volume with a high relative biological effectiveness (RBE), cancer cells can be significantly damaged while causing minimal toxicity to surrounding healthy cells. Recent clinical studies have given encouraging results for targeted alpha-particle therapy (TAT) in the treatment of metastatic, castration-resistant prostate cancer and the number of promising radiopharmaceuticals for clinical TAT is growing rapidly [15, 16]. However, while it has been a long-standing research goal, the majority of the Auger electron emitter therapy studies still remain preclinical [10]. Both α-particle and Auger electron emitters are considered as high LET radiation qualities; with an LET of 80–100 keV/μm for α-particle emitters and an LET of 4–26 keV/μm for Auger electron emitters [15]. As a result, the path length of Auger electrons is much shorter compared to α-particles, typically <0.5 μm [16]. Another important difference is the lack of a cross-fire effect for Auger electron emitters. For α-particle emitters on the contrary, recent studies did observe a significant therapeutic effect on large tumors, pointing in the direction of a cross-fire effect [17, 18]. In the situation of DNA-associated decay, the RBE of Auger electrons is very similar to α-particles. The main challenge for Auger emitter therapy remains the requirement to target the radioisotope into individual tumor cells and more specifically, into the nucleus of those cell. On the other hand, this makes Auger emitters even more appealing, since they have a lower toxicity when they decay outside the cell nucleus (e.g., cytoplasm or outside cells), in contrast to α- and β-particle emitters [8, 19]. However, a growing body of evidence suggests that internalization in the cell nucleus is not obligatory for Auger electron emitters to induce cell killing, although the cytotoxic effect is less prominent than in the case of nuclear DNA targeting [20, 21].

Since nuclear localization seems to be of critical importance for the efficacy of Auger emitter therapy, several labeling methods and experimental approaches have been tested in the past decades in order to target Auger emitter to the nucleus of cancer cells [6]. More recent radiolabeling efforts are focused on monoclonal antibodies or peptides that recognize cell surface receptors displayed on cancer cells [22]. However, most of the pioneering work has come from using radiolabeled iododeoxyuridine, in particular with ^{125}I- or ^{123}I-5-iodo-2-deoxyuridine (IUdR) [16]. These thymidine analogues are directly incorporated into cellular DNA during the synthesis-phase (S-phase) of the cell cycle and provide one of the most reliable methods for the experimental measurement of the radiobiological effects of these nanometer range Auger emitters [10]. The dependence on the synthesis phase of the cell cycle for the incorporation poses a restriction to *in vivo* applications, but it is still very useful for *in vitro* proof of principle studies.

While ^{125}I is one of the more commonly used radioisotopes to study *in vivo* and *in vitro* Auger electron induced DNA damage, ^{123}I was chosen for this study. Despite the fact that it only releases about 14% of its decay energy in the form of Auger electrons, its relatively short half-life of 13.2 h makes it possible to deposit biologically detectable quantities of radiation energy over a short period of time. It makes this radioisotope also a good candidate for therapy, since this half-life would adapt well for peptide or oligonucleotide labeling and the biodistribution could be followed by scintigraphy based on the 159 keV γ-radiation [10]. The relatively long half-life of ^{125}I (59.4 days) would require exposing the cells to the isotope for weeks to accumulate enough disintegrations that result in detectable levels of biological damage. Using such long lived isotopes requires cryogenic freezing of *in vitro* cell samples in a mixture containing dimethyl sulfoxide (DMSO). The latter is a free radical scavenger with radio-protective properties and previous studies have shown a significant reduction in biological effects of DNA-bound Auger emitters in the presence of DMSO, pointing to the importance of indirect effects [23]. Therefore, it was decided to use ^{123}I in this study, so the cell samples could be

exposed to the radionuclide under normal physiological conditions.

The short range of the Auger electrons coincides with the 2 nm diameter of the DNA helix, since the typical high LET Auger emitter cascade will deposit its highest energy in a range of 1–2 nm [24]. Therefore, it is generally accepted that one decay of ^{125}I and ^{123}I associated with the DNA, will result in one DNA double-strand break (DSB). In addition, Auger electron emitters also damage the cells indirectly via the radiolysis of water and the production of free radicals, such as reactive oxygen species (ROS). More recently, several studies have investigated the non-targeted effect of Auger-electron emitters, known as bystander effects, on more distant cells [25–27]. Previous studies which made use of ^{125}I- and ^{123}I-iododeoxyuridine (IUdR) measured RBE values of 8 and 7 respectively in Chinese hamster V79 lung fibroblasts [24, 28]. It has been demonstrated by several authors that Auger electron emitters will cause complex and multiple DSB to the DNA via direct interaction or through the ROS production [29, 30], which can result in cell death if unrepaired or chromosomal aberrations in the case of misrepair [31–33]. The induction of complex DNA damage that challenges the cells' repair capacity, is generally accepted to be the underlying mechanism of the high genotoxic potential of Auger emitters. However, a recent study by Schmitz et al. highlighted that only a limited number of studies are available on chromosomal aberrations induced by Auger emitters [32]. In their study, the authors illustrated a strong genotoxic effect on ^{125}IUdR, even at a low dose of 0.2 Gy, by analyzing chromosomal aberrations and apoptosis in human peripheral blood lymphocytes for the first time [32]. To the best of our knowledge, similar *in vitro* data on ^{123}IUdR is not available yet, however Hindorf et al. did establish the feasibility of treating B-cell lymphoma with internalized ^{123}I or ^{125}I using Monte Carlo dosimetry calculations [34, 35]. In the current study, the micronucleus assay was used since it is considered to be one of the most reliable methods to determine chromosome damage as it enables the measurement of both chromosome loss and chromosome breakage. Micronuclei (MNi) are small extranuclear bodies resulting from chromosome breaks. The cytokinesis-block micronucleus (CBMN) assay is the preferred method to measure MNi in genetic toxicology testing, since it restricts the scoring to once-divided binucleated (BN) cells. This BN appearance is obtained by adding cytochalasin-B (Cyto-B) to the cell cultures, which inhibits the completion of cytokinesis. Restricting the scoring of MNi to these BN cells prevents confounding factors due to suboptimal or altered cell division kinetics [36]. Over the years, the CBMN assay has proven to be a very reliable, thoroughly validated and standardized technique in the field of radiation biology to evaluate *in vivo* radiation exposure of occupational, medical and accidentally exposed individuals and to assess individual *in vitro* radiosensitivity or cancer susceptibility [37].

Dosimetry calculations are needed in order make a good interpretation of the radiobiological effects caused by an internally distributed radionuclide and to allow comparison with the effects observed with an external beam source. Early attempts to determine the absorbed dose used semi-analytical methods according to the MIRD schema [38, 39]. Monte Carlo methods have been used to overcome the limitations of analytical methods in describing the transport of low energy charged particles at the cellular level [40–42]. Direct comparisons of radionuclide microdosimetry are complicated since different radionuclide emission spectra, particle interaction cross section tables, low-energy physics models, simulation geometry and other approximations are employed by the different Monte Carlo codes. In this work, we employ the open-source and well-documented Geant4-DNA Monte Carlo toolkit which has been widely used for nano- and microdosimetric applications [43], and previously described in [44]. The ^{123}I-iododeoxyuridine (^{123}IUdR) was synthesized to carry ^{123}I across the cell membrane and be incorporated into synthesizing DNA. Human lymphocytes were used in this study, which reside predominantly in the G0 phase, the DNA pre-synthetic stage of the cell cycle. Therefore, lymphocytes were stimulated to undergo *in vitro* mitoses using phytohemagglutinin (PHA) in order to push the cells into the S-phase and allow maximum incorporation of ^{123}IUdR. As previously mentioned, chromosomal damage was evaluated with the CBMN assay and RBE values were calculated at several levels of biological effect as well as RBE_{Max} by comparison with ^{60}Co γ-ray irradiations.

MATERIALS AND METHODS

Synthesis of ^{123}I-Iododeoxyuridine

All reagents were received from commercial sources (Sigma-Aldrich, Merck South Africa) and were used without further purification. All reactions were performed under a nitrogen atmosphere; unless otherwise stated. ^{123}IUdR synthesis was performed using a modified protocol from that of Uddin et al. [45]. Hexabutylditin (200 μL) was added to a solution of 5-iodo-2′-deoxyuridine (50.0 mg) and tetrakis (triphenylphosphine) palladium (0) ($Pd(PPh_3)_4$) (7.00 mg) in anhydrous dioxane (3 ml) and heated at 100°C for 18 h. The reaction progress was monitored by thin layer chromatography (TLC) using aluminum backed silica-gel 60 F-254 plates (Merck, South Africa) and was observed using both ultraviolet and fluorescent light. Following completion, the reaction mixture was cooled to room temperature, concentrated under vacuum and subjected to flash chromatography using Kieselgel 60 silica gel (Sigma, South Africa), hexane and ethyl acetate to afford 5-(tributylstannyl)-2′-deoxyuridine (48.2 mg, 67%) as a yellow oil.

Synthesis of ^{123}IUdR, 2

5-(Tributylstannyl)-2′-deoxyuridine (0.50 mg) and $Na^{123}I$ (8 μL, ^{123}I produced *via* the ^{127}I (p, 5n) ^{123}Xe cyclotron reaction and recovered as no-carrier-added $Na^{123}I$ in 0.01 M NaOH solution) were reacted at room temperature in the presence of *N*-chlorosuccinimide (1.00 mg) in a (1:2) DMSO: phosphate-buffered saline (PBS) solution for 20 min. The reaction was then quenched by the addition of an aqueous solution of sodium thiosulfate (0.5 mg) in deionized water (0.5 ml). The quenched mixture was further diluted with deionized water (2 ml) and loaded on a pre-conditioned (3 ml methanol; 2 ml

deionized water) reversed phase C18 mini-cartridge (500 mg C18, 3 cc, Sep-Pak, Waters, United States). Elution was carried out with the eluent composed of 5% ethanol in 95% deionized water with a flow rate of 1 ml/min, at $\lambda = 254$ nm and produced a peak at $t_r = 17.1$ min on a high-performance liquid chromatography (HPLC) C18 column (250 mm × 4.6 mm, 5 μm) (Phenomenex Luna, United States). The radiochemical content of the labeled product was determined using a CsI (Tl) radioactivity detector (Carroll and Ramsey Model 105S-1). The radioactivity content of ^{123}IUdR constituted approximately 52.9 MBq (or 1.43 mCi), was further diluted to 2.00 ml of 5% ethanol in water. The collected fraction of ^{123}IUdR was diluted in Roswell Park Memorial Institute (RPMI) medium (Gibco, ThermoFisher, South Africa), supplemented with 10% fetal calf serum (Lonza, South Africa) and 1% penicillin and streptomycin (Lonza, South Africa) to a final activity concentration of 26.5 MBq/mL.

Blood Sample Collection and Experimental Conditions

The ethics approval for the study was obtained from the Human Research Ethics Committee at Stellenbosch University (reference number: S12/04/091). Blood samples were collected by venipuncture from three male adult volunteers (25–50 years), from whom informed consent was obtained prior to the experiments. Blood samples were collected in lithium-heparin collection tubes and peripheral blood mononuclear cells (PBMCs) were isolated from whole blood using density gradient cell separation medium (Histopaque-1077, Merck). The PBMCs were counted and suspensions of approximately 1×10^6 cells/1.00 ml were pipetted into a 15 ml round bottom tube. Samples were divided for irradiations with ^{60}Co γ-rays and the labeling with ^{123}IUdR. Each sample set included a sham-irradiated control sample. For all radiation exposure conditions, lymphocytes were stimulated to divide in culture using phytohemagglutinin (PHA, 1 mg/ml) and kept at 37°C in a humidified 5% CO_2 incubator for 48 h.

Thereafter, the cell suspensions from each donor were exposed to graded doses of ^{123}IUdR (0, 0.19, 0.37, 0.56, 0.74, 0.93, 1.9, and 3.7 MBq) diluted in culture medium at 37°C. After a 1 h pulse labeling, samples were washed (two times) with cold PBS to remove excess ^{123}IUdR that was not incorporated into the cell. The radioactivity levels were then measured in a 3-inch well type NaI (Tl) scintillation detector (CANBERRA model 802 series) that was coupled to a multi-channel analyzer (Silena). The Silena EMCA 2000 software was used to collect the characteristic γ-ray emissions of ^{123}I at 159 keV. The readings were corrected for detector efficiency, photo-peak abundance, and decay. After readings were completed, the culture tubes were left at room temperature for 24 h in order to accumulate radiation damage. After these 24 h, the cell pellet was resuspended in fresh complete RMPI medium containing PHA (1mg/ml, Sigma Aldrich, South Africa) and cytochalasin B (6mg/ml, Sigma Aldrich, South Africa) at 37°C in a humidified 5% CO2 incubator for 24 h.

For the cultures irradiated with ^{60}Co γ-rays, the isolated, stimulated lymphocytes were exposed to graded doses of 0, 0.5, 1, 2, and 4 Gy. Cell suspensions were placed between a 5 mm thick sheet of Perspex (build-up) and 50 mm backscatter material with a dose rate of 0.49 Gy/min for a 300 mm × 300 mm field size at 750 mm Source to Surface Distance (SSD). Thereafter, cytochalasin B (6mg/ml, Sigma Aldrich, South Africa) was added and cultures were incubated for a further 24 h.

Cytokinesis Block Micronucleus Assay

After exposure to either ^{60}Co γ-rays or ^{123}IUdR, the cell cultures were harvested at total culture time of 72 h. This involved washing the pelleted sample with a cold hypotonic KCl solution (0.075 M). Samples were then washed using methanol: acetic acid: ringer fixative solution (10:1:11) and stored at 4°C overnight. Samples were then washed with methanol: acetic acid (10:1) solution. Thereafter, concentrated cell suspensions were dropped on clean microscope slides and stained with acridine orange. For each sample, approximately 500 binucleated lymphocytes were manually scored using a fluorescent microscope (Zeiss, Axio Imager A1) at 20× magnification. At least 3 slides were analyzed per exposure condition and the average number of micronuclei per 500 BN cells was calculated for each condition.

S-phase Fraction Determination

The ^{123}IUdR incorporation in the DNA of the lymphocytes depends on the fraction of cells that goes through the S-phase of the cell cycle. Therefore, flow cytometry was used in this study to determine the number of cells which were in S-phase at the time they were labeled with ^{123}IUdR. Two lymphocyte cultures (one stimulated by PHA and one non-stimulated) from each donor were used for this purpose. A bromodeoxyuridine (BrdU) kit (BD Pharmingen, Germany) was used to detect active DNA synthesis, through antibody-based staining of BrdU, together with total DNA content based 7-AAD staining. BrdU is a synthetic nucleoside and well-known thymidine analogue, which can be incorporated into newly synthesized DNA of replicating cells during S-phase. This staining technique makes it possible to clearly separate cells in G1 from early S-phase, or late S-phase from G2/M [46]. The non-stimulated culture was used to determine the background counts which should be subtracted from the stimulated culture. Briefly, cells were stimulated with PHA as described previously, pulse labeled with BrdU for 1 h and analyzed after 48 h in culture. The cultures were fixed and permeabilized using the BD Cytofix/Cytoperm buffer and incubated with DNase for 1 h at 37°C. Thereafter, the samples were washed with the BD Perm/Wash buffer and incubated with the anti-BrdU antibody for 20 min at room temperature in the dark. The samples were washed again and total DNA was stained using 20 uL 7-AAD, resuspended in about 1 ml of the provided staining buffer and events acquired using the BD Accuri C6 Flow cytometer ((BD, Becton Dickinson and Company, San Jose, United States).

Determination of the Absorbed Dose (MBq to Gy)

The Geant4 Monte Carlo toolkit was used to calculate the dose delivered to the cells by the incorporation of ^{123}I into the cellular DNA as previously described in [44]. The dosimetric calculations for these *in vitro* experiments with ^{123}IUdR involved converting the energy imparted by the incorporated activity A_0 in a mass M of cells into an absorbed dose value *D*. The absorbed dose is defined as the mean energy imparted $\bar{E}$ by ionizing radiation to matter of mass m in a finite volume V by $D = \bar{E}/m$.

The mass of a spherical shape, $m = \rho V = 4/3\pi r^3$, can be obtained using the density and the volume, or the radius if it is known.

The dependence of the dose absorbed on the size and geometry of the cell is clear from the definition of absorbed dose. For this reason, experimental measurements of the diameters of isolated and stimulated lymphocytes were made using light microscopy and a calibrated imaging system. The total number of intra-nuclear decays during the 24 h period could be derived by integration of the experimentally obtained average incorporated radioactivity [47]. ^{123}I has a half-life τ of 13.2 h (the decay constant $\lambda = Ln\ (2)/t$. The activity at a time t is given by:

$$A(t) = A_0 e^{-\lambda t} = A_0 e^{-\ln(2)t/\tau} \quad (1)$$

The number of disintegrations after a time Δt would then be given by:

$$N(\Delta t) = \int_0^{\Delta t} A(t)dt = \frac{A_0 \tau}{\ln(2)}\left[1 - e^{-\ln(2)\Delta t/\tau}\right] \quad (2)$$

As described by Makrigiorgos et al., the cumulated radiation dose to the cells may be calculated by using the total number of decays, the average $\overline{E}$ energy deposited in the cell per decay, and the cellular dimensions [28]. Sefl et al. concluded that under relevant clinical conditions, the uptake rate of the radiopharmaceutical is an important additional factor that needs to be considered in radiobiological models of cell survival in targeted radionuclide therapy [48]. In our study, the incorporated activity A_0 was measured experimentally in the cell pellet using a 3-inch well type NaI-scintillation detector. To improve the radionuclide uptake, the ^{123}IUdR was introduced to the lymphocytes 48 h after stimulation, when a large percentage of the cells would be in S-phase. To further prevent additional radionuclide uptake, the residual activity was washed out and cold medium was used to prevent further division. Therefore, the uptake rate as defined by Sefl et al. was not taken into consideration in the dose calculations that were performed as part of this study. Following from equation [2] the absorbed dose in the mass M of cells is determined by:

$$D\,[Gy] = \frac{N(\Delta t) \cdot \overline{E} \cdot 1.6 \times 10^{-19}}{M} \quad (3)$$

The average energy $\bar{E}$ deposited in a cell per decay was obtained from Monte Carlo simulations using the Geant4-DNA toolkit and described in Fourie et al. [44]. The Geant4-DNA extension of the Geant4 Monte Carlo toolkit simulates electron tracks and their energy deposition, collision-by-collision, down to the excitation threshold of liquid water (7.5 eV); opposed to other MC codes like MCNP or EGS which are limited down to 1 keV. In the study by Fourie et al., spheres of unit density water were used to represent a cell and its nucleus in suspension. The G4EmDNAPhysics physics list and Livermore models were used to describe all particle interactions during the simulation. The G4RadioActiveDecayPhysics class along with the built in ENSDF emission data from Brookhaven National Laboratory was used to simulate the radioactive decay of ^{123}I and resultant x-ray and electron emissions. Readers are referred to [49] for more details.

The mass M in which the cumulative energy is deposited is obtained from the mass of total number of cells seeded per culture, corrected by the S-phase fraction. Sefl et al. investigated the effect of cell geometry on S-values (energy deposited per unit activity) using the Geant4 Monte Carlo toolkit with the Geant4-DNA low-energy extension [50]. For the ^{125}I radionuclide they found the S-values of the commonly used spherical geometry corresponded within 5% to ellipsoid geometries when the radionuclide was distributed within the cell. For the most oblong ellipsoid, the dose to the nucleus was 22% less compared to the spherical geometry when the radionuclide was distributed in the cytoplasm. Similarly to Fourie et al. [44], they found the dose to the nucleus was a factor of 10 less when the radionuclide was distributed outside of the nucleus. The S-phase fraction attempts to approximate the number of cells in the sample which incorporated the ^{123}I into the nucleus.

Relative Biological Effectiveness

The resulting radiation-induced chromosomal damage is expressed as the number of MNi per 500 BN cells. This value was then plotted against the absorbed dose and a dose-response curve was fitted to the data points. For low-LET radiation (e.g., ^{60}Co γ-rays) the curve usually had the linear-quadratic form, which can be described as $y = c + \alpha D + \beta D^2$. Here, y represents the number of micronuclei (per 500 BN cells) induced by a dose D. The background MNi frequency of each donor *c* (obtained from the control sample which was not exposed to radiation) is subtracted from each data point before the line fitting is done, resulting in $y = \alpha D + \beta D^2$. For high-LET radiation, the α-term becomes large and eventually the β-term becomes biologically less relevant and also statistically "masked" such that the dose response is approximated by a linear equation.

The RBE is expressed as the ratio of the absorbed doses of a low-LET reference radiation quality (e.g., 250 kV X-rays or ^{60}Co γ-rays) to a test radiation quality which produce the same level of biological effect (i.e., in this specific study: the doses $D_{Co\text{-}60}$ and $D_{I\text{-}123}$ which produce y MN). The dose producing the effect y can be determined by solving for D in the fitted dose-response curves.

$$RBE = \frac{D_{Co-60}}{D_{I-123}} = \frac{D_{\text{linear-quadratic}}}{D_{\text{linear}}} = \frac{-\alpha_{Co-60} + \sqrt{\alpha_{Co-60}{}^2 + 4\beta y}}{2\beta} \div \frac{y}{\alpha_{I-123}} \quad (4)$$

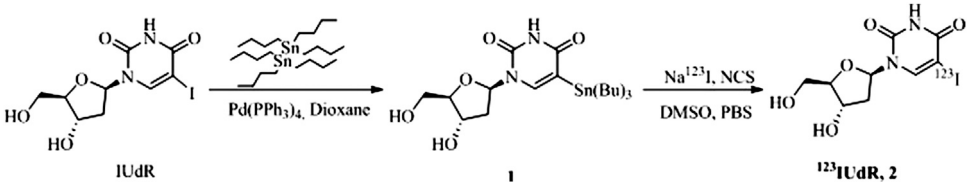

FIGURE 1 | Synthesis and labeling scheme of ^{123}I-iododeoxyuridine, 2.

The RBE value is dependent on the spatial distribution of the energy imparted, the density of ionizations per path length of ionizing particles and the reference radiation. The IAEA TRS 405 and the ICRP-ICRU RBE Committee defined two representative RBE values: the maximum value of relative biological effect (RBE_{Max}) and the minimum relative biological effect (RBE_{Min}) [51, 52]. RBE_{min} is the RBE at very high doses; whilst RBE_{Max}, also known as the dose limiting RBE, is the RBE at near zero dose and can be represented by the ratio of the initial slopes (α–values) of the dose-effect curves for the studied radiation and the reference radiation:

$$RBE_{Max} = \frac{\alpha_{I-123}}{\alpha_{Co-60}} \quad (5)$$

Statistical Analysis

Data presented includes the mean number of MN ± standard deviation where applicable and radioactivity levels of independent experiments on different days. Statistical analysis and curve fitting were performed using GraphPad Prism Software Version 5.00 for Windows. Results were considered to be statistically significant at $p < 0.05$.

RESULTS

Radiolabeling of ^{123}I-Iododeoxyuridine

The radiolabeling of IUdR (**Figure 1**) was achieved by first producing a tin intermediate by heating 5-iodo-2′-deoxyuridine with hexabutylditin and tetrakis (triphenylphosphine) palladium (0) ($Pd(PPh_3)_4$) in anhydrous dioxane for 18 h [45]. The tin intermediate was produced via the palladium-catalyzed metal-halogen exchange reaction, whereby the palladium (0) catalyst is oxidatively added to the carbon-iodine bond, followed by transmetallation of one of the tin groups to the palladium center with removal of bromotributyltin [53]. The reaction progress was monitored by thin layer chromatography (TLC) and once the reaction was completed, the reaction mixture was subjected to column chromatography using ethyl acetate and hexane as mobile phase to isolate **1** as a yellow oil in 67% yield. The structure was confirmed using high performance liquid chromatography (HPLC) and ^{1}H NMR (proton nuclear magnetic resonance) spectroscopy. Then, ^{123}IUdR, **2**, was successfully synthesized by adding $Na^{123}I$ to a solution of **1** and *N*-chlorosuccinimide in DMSO and PBS for 20 min at room temperature. The reaction was stopped by the addition an aqueous solution of sodium metabisulfite to quench any iodine in the reaction mixture. Thereafter, purification was done by reverse phase HPLC using a solution of 5% ethanol in deionized water to obtain **2** with approximately 52 MBq (or 1.4 mCi) radioactivity.

Incorporation of ^{123}I-Iododeoxyuridine

The ^{123}IUdR incorporation into DNA of isolated lymphocytes is dependent on the fraction of cells that goes through the synthesis phase of the cell cycle. Cell cycle analysis was performed with flow cytometry to determine the percentage of cells that were in S-phase during pulse-labelling with ^{123}IUdR. Two lymphocyte cultures of approximately 1 × 106 cells each (one stimulated by PHA and one non-stimulated) were used from each donor to determine the S-phase fractions. The non-stimulated culture served as the background count which was subtracted from the stimulated culture. After subtraction, the fraction of lymphocytes which incorporated BrdU was found to be approximately 22% for donor 1, 22% for donor 2, 13% for donor 3. The residual radioactivity that was measured after the different wash steps is presented in **Figure 2** for donor 3 after 1 h pulse-labelling with ^{123}IUdR. This clearly illustrates that stimulated lymphocytes could incorporate ^{123}IUdR more effectively than their non-stimulated counterparts. Comparing the slopes of the fitted trend-lines, the average uptake of ^{123}IUdR at different activity levels increased by a factor of 2 due to the addition of PHA.

^{123}I-Iododeoxyuridine Dose Response Curve

The lymphocyte samples were exposed to concentrated solutions containing ^{123}IUdR, washed with cold PBS and residual radioactivity levels were measured in a well type sodium iodide scintillation detector. These measured activities were converted to absorbed dose (Gy) as described in a previous publication using equation [3, 44]. The International Atomic Energy Agency reports that peripheral lymphocytes 48 h after stimulation have a cell volume of about 500 μm^3. Using a calibrated image analysis system, an average cell diameter for our isolated and stimulated lymphocytes was found to be 9.8 ± 1.7 μm (~486 μm^3). Therefore, in the absorbed dose calculations, a cellular diameter of 10 μm and a nuclear diameter of 8 μm were assumed. The resulting absorbed dose and associated induced MNi per 500 BN cells are presented in **Table 1** for the three donors.

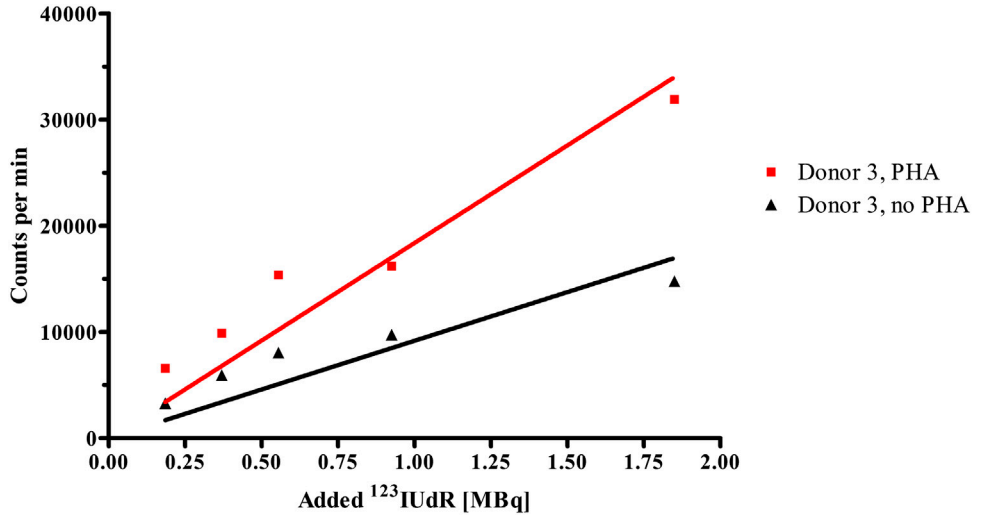

FIGURE 2 | Radioactivity levels incorporated by stimulated (PHA) and non-stimulated (no PHA) lymphocyte cultures of Donor 3 after the 1 h pulse-labelling with 123IUdR activities.

The ^{123}IUdR activity levels resulted in a higher absorbed dose for donor 3, compared to donors 1 and 2, while the S-phase fraction of donor 3 was only 13%. The higher absorbed dose value might be attributable to the fact that a different synthesis batch was used for donor 3, while donor 1 and 2 came from the same batch. Therefore, it is suspected that the new batch had a higher labeling efficiency, thereby leading to an increase in uptake for donor 3 per added activity.

A linear relationship between micronuclei frequency and ^{123}I activity (converted to absorbed dose values) could be established, as shown in **Figure 3**. The background counts are subtracted from the individual dose points, hence the linear fit intercepts the origin. The lowest activity level of 0.19 MBq ^{123}IUdR did not induce a significant increase in MNi compared to the background MNi frequency of each donor ($p = 0.24$), but a significant increase was observed from 0.37 MBq ^{123}IUdR onwards ($p < 0.05$). The MNi frequencies induced by the higher dose points (>1 Gy) deviate significantly from a linear response. This under-response could be a characteristic of cell death or mitotic delay due to the high biological effectiveness of Auger electrons. Therefore, these higher dose points were not taken into account for the linear fit presented in **Figure 3**. In addition, the 1.85 MBq of ^{123}IUdR activity induced a very high level of MNi for donor 2 (207 MNi/500 BN cells). This point was considered as an outlier and not included in the fitting.

Dose Response Curve Donor After ^{60}Co Dose Response Curve

In order to determine the biological effectiveness of the ^{123}I Auger electrons, lymphocytes from the same donors were exposed to a reference radiation quality, ^{60}Co γ-rays, with graded doses ranging from 0.5 up to 4 Gy. The observed number of MNi per 500 BN cells for each donor were plotted against the dose, which resulted in the characteristic linear-quadratic dose-response curves for low-LET radiation for each donor, as shown in **Figure 4**. Again, the induced MNi frequencies were plotted, where the background counts from the sham-irradiated controls were subtracted for each dose point. **Table 2** shows the α- and β-values obtained from the linear-quadratic curves as

TABLE 1 | The mean absorbed dose (Gy) and mean micronuclei (per 500 BN cells) induced following exposure to different levels of ^{123}IUdR activity.

^{123}IUdR added (MBq)	Donor 1		Donor 2		Donor 3	
	Gy	MN	Gy	MN	Gy	MN
0	0	43 ± 7	0	36 ± 7	0	82 ± 16
0.19	0.16 ± 0.02	44 ± 10	0.05 ± 0.01	45 ± 13	0.18 ± 0.02	107 ± 28
0.37	0.10 ± 0.02	69 ± 9	0.14 ± 0.02	72 ± 17	0.26 ± 0.02	138 ± 18
0.56	–	–	–	–	0.55 ± 0.05	156 ± 2
0.74	0.17 ± 0.02	84 ± 10	0.13 ± 0.02	79 ± 16	–	–
0.93	–	–	–	–	0.92 ± 0.08	210 ± 28
1.85	0.57 ± 0.05	116 ± 17	0.27 ± 0.05	207 ± 27	1.41 ± 0.13	190 ± 23
3.70	1.85 ± 0.16	137 ± 27	1.56 ± 0.14	154 ± 22	–	–

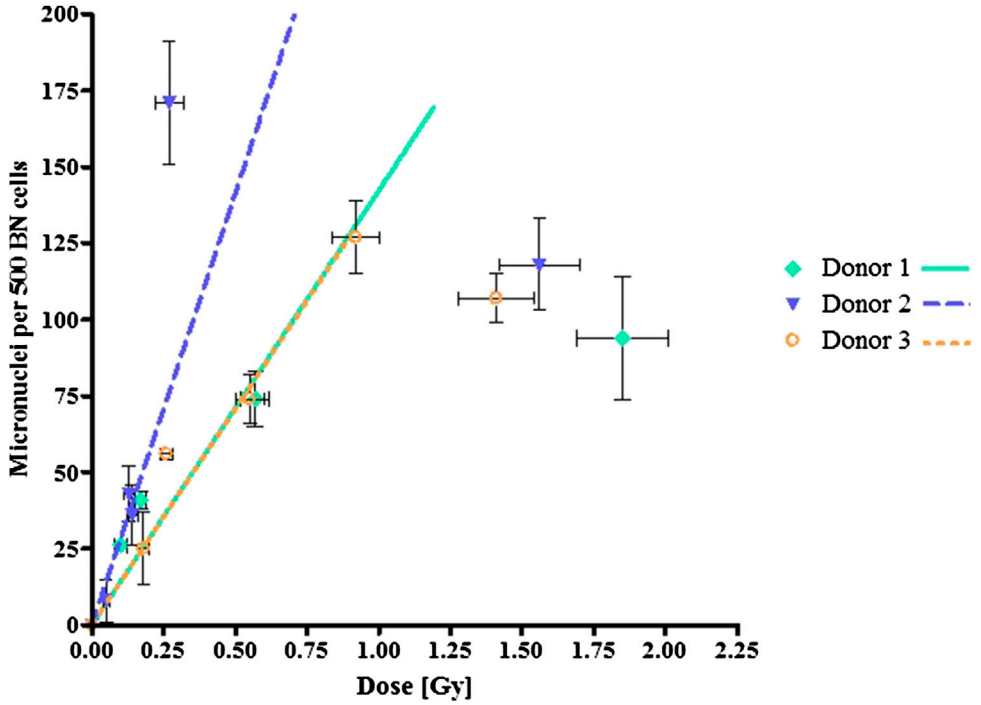

FIGURE 3 | Dose-response curves following exposure to 123IUdR activities presenting micronuclei formation as a function of absorbed radiation dose (Gy). The error bars are the standard deviations of the mean micronuclei frequency/500 BN cells for each dose point.

described in **Eqs 4** and **5**. The α-values for the Auger emitter are significantly greater than that of the reference radiation, indicating that the lymphocytes are more radiosensitive to the Auger electron emitter thereby causing more biological damage than the ^{60}Co reference radiation quality.

The Relative Biological Effectiveness

Using the fitted curves obtained from the ^{123}I and ^{60}Co experiments with the same donors, the RBE was calculated using equations [4] for each ^{123}I dose point reported in **Table 1** (which induces a specific number of MNi, i.e. the biological effect). In this way, a range of RBE values was obtained for each donor, depending on the dose under investigation. This calculated RBE range is given in **Table 3** and visually presented in **Figure 5**. The dose-limiting RBE (RBE_{Max}) was obtained from the α-values of the fitted dose-response curves as outlined in equation [5] and is also listed in **Table 3**.

As shown in **Figure 5** the RBE plateaus for each donor, reaching RBE_{Min} values between 3 and 5, suggesting that above a certain dose level, the relative effectiveness of the Auger electrons to induce a certain response remains constant. Much larger RBE values were observed at the radiation doses below 0.1 Gy, particularly for donor 1 and 2 (see **Figure 5**). This observation is in line with the general rule that RBE values increase with decreasing dose. Based on our findings, it seems that the variation in the RBE values for the different donors is much more pronounced at low doses. This could be indicative of donor specific cellular response at low doses. In addition, a rather large variation was observed in RBE_{Max} values, where the dose limiting RBE for donor 3 was almost half the value of donor 1 and 2.

DISCUSSION

Owing to the ability of Auger electron emitters to deposit their energy in an extremely small volume, typically in the range of cubic nanometers, Auger electron emitters are now increasingly considered for therapeutic purposes [54]. There are few satisfying vectors available for specifically targeting the nuclear DNA of cancer cells; historically antibodies or peptides are used to target cancer cell membranes but, following internalization in the cells using these vectors, the transport from the cytoplasm to the nucleus is one of the key stages in the delivery of Auger emitter therapy as recently described by Rosenkranz et al. [55]. The number of pre-clinical studies with Auger electron emitters is growing, which is illustrated in two very recent publication with the ^{123}I-Meitner-Auger PARP1 inhibitor (^{123}I-MAPi) and a small-molecule Auger electron emitter targeting the prostate-specific membrane antigen (PSMA) [56, 57]. ^{123}I-MAPi the first Auger-based theranostic PARP inhibitor able to directly deliver its lethal damage in the DNA of glioblastoma cells [56]. The isotope ^{123}I is an ideal candidate for targeted radionuclide therapy, due to its Auger decay and the opportunity to simultaneously image the tumor with SPECT imaging based

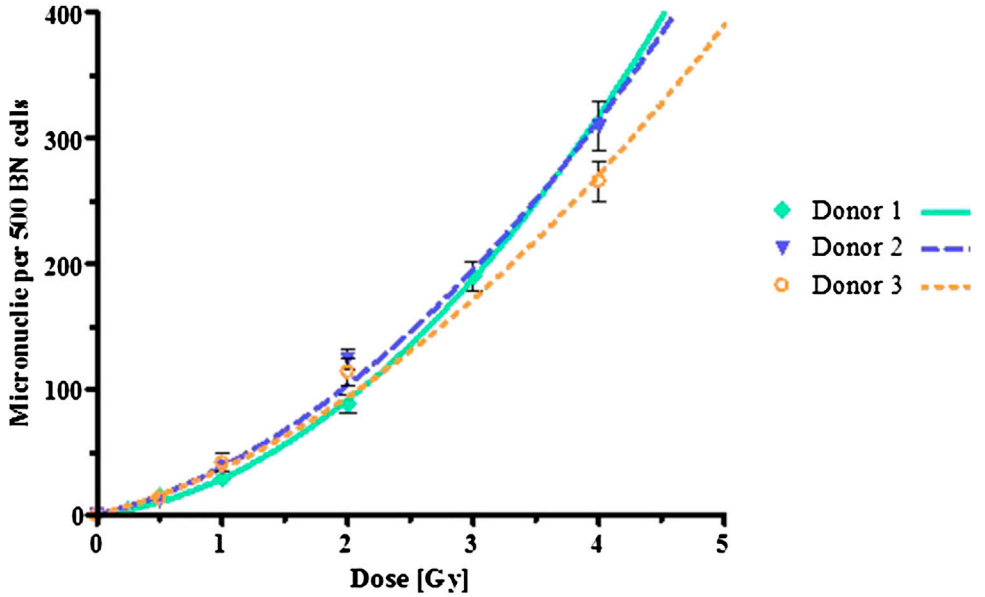

FIGURE 4 | Dose-response curves following exposure to ^{60}Co γ-rays radiation. The error bars are the standard deviations of the mean micronuclei formation per dose point.

on its characteristic 159 keV γ-ray, which provides the option to calculate dosimetry and treatment efficacy. However, ^{123}I is less often studied compared to its ^{125}I counterpart for radiobiology investigations and therefore, information on the RBE of the Auger emitter ^{123}I remains limited. This study aimed to add to the evidence of the high-LET characteristics of this radionuclide, by using ^{123}IUdR incorporated in the DNA of lymphocytes of healthy adult volunteers in order to get a better understanding of the induced chromosomal damage and respective RBE values. When comparing the dose response curves obtained with ^{60}Co γ-rays and ^{123}IUdR Auger electrons, RBE values ranging from 3 to 10 were observed, depending on the radiation dose and the donor.

The CBMN assay was used to estimate the radiation damage in this study, instead of the dicentric and chromatid aberration assays that were previously used by other research group to investigate the biological effects of Auger emitting isotopes [32, 58–60]. As outlined in a study of Slabbert *et al.* on inter-donor variations in radiosensitivity to high- and low-LET radiation, the CBMN assay is a useful endpoint for RBE studies that involve high-LET radiation qualities [61]. The radiation-induced MNi stem from acentric chromosome fragments that are directly associated with dicentric formations [62]. In addition, the fact that lymphocytes present a synchronous population of resting G0 cells at the start of the experiments, with a uniform radiosensitivity, is an advantage compared to cell lines which are distributed in different phases of the cell cycle. The work of Slabbert *et al.* used the same CBMN method on lymphocytes of four different donors to illustrate that variations in the RBE_{Max} of high-LET radiation, namely fast p (66)/Be neutrons (29 MeV), differ due to a different inherent radiosensitivity to low-LET radiation [61]. Therefore, dose-response curves of ^{60}Co γ-rays, generally accepted as the reference radiation quality for RBE calculations, of the same donors were included in this study. From the sets of lymphocyte data of the three donors, a slight inter-donor variability in the dose-responses to ^{60}Co γ-rays was noted, being indicative for the inherent radiosensitivity, which was also observed by Vral et al. [63]. A linear relationship between micronuclei frequency and ^{123}I activity could be established as shown in **Figure 3** for all donors. In general, even low doses of approximately 0.15 Gy of ^{123}I already induced a significant increase in chromosomal damage. Furthermore, it was observed that the higher dose points deviated significantly from linearity. This stunted response might be attributable to a critical amount of lethal damage or a G2/M cell cycle arrest at the higher damage,

TABLE 2 | Slopes of the fitted curves for ^{123}IUdR and ^{60}Co γ-ray exposures. The α- and β-values correspond to the linear-quadratic curve fitting.

—	Donor 1		Donor 2		Donor 3	
	α [Gy^{-1}]	β [Gy^{-2}]	α [Gy^{-1}]	β [Gy^{-2}]	α [Gy^{-1}]	β [Gy^{-2}]
^{123}I	142.3 ± 21.3	–	282.8 ± 27.7	–	141.9 ± 8.7	–
^{60}Co	12.3 ± 3.2	16.8 ± 1.2	25.0 ± 9.7	13.4 ± 2.7	26.4 ± 9.5	10.4 ± 2.7

TABLE 3 | The RBE ranges and RBE_{Max} values for ^{123}I as test radiation and ^{60}Co as reference radiation.

Donor	RBE range	RBE_{Max}
1	3 ± 1 to 9 ± 2	11 ± 3
2	5 ± 3 to 10 ± 4	11 ± 4
3	3 ± 3 to 4 ± 3	5 ± 2

which limits the number of viable or BN cells expressing MNi for scoring. However, this plateau was not observed in the linear fit of Schmitz *et al.* for chromosomal aberrations after exposure to ^{125}IUdR [32]. In the current study, the higher dose points were not taken into account for the linear fit. The observed plateau in our study indicates that the type of DNA damage caused by ^{123}IUdR is structurally more complex and therefore comparable with clustered high LET-type damage, which challenges the DNA damage repair machinery of the cells [29]. Another explanation for the observed plateau effect might be attributable to bystander effects, which are estimated to contribute approximately 30% to the total cell killing effect of Auger electron emitters [27]. In this study, the uptake at the higher radioactivity level might have been inferior, meaning that the observed plateau is coming from the bystander effect which might be less dose dependent compared to the direct cell killing effect. While there is no reason to assume that the uptake at 3.7 MBq did not increase compared to 1.85 MBq in our study, further investigations on the contribution of direct and bystander effects to the MN results could be interesting.

As previously mentioned, the attempts to use Auger emitters as cancer therapy have been hindered by the limited range of the emitted radiation and the difficulty of reliably deliver the electron close enough to the DNA target [64, 65]. The short range of Auger emitters makes them advantageous for disseminated cells and metastasis, but for larger solid tumors, a larger number of Auger electron emitting radionuclides might be needed to obtain the same level of cytotoxic effects as cross-firing β-emitters. This was previously illustrated in a study where tumor bearing rats were exposed to ^{111}In-octreotide peptide receptor radionuclide therapy, where a complete response was observed in rats with a small (<1 cm^3) tumors, but only partial regression was observed in rats with larger lesions [66]. The short range of most Auger electron emitters requires a very close proximity to the DNA. Therefore, it was decided to use a carrier molecule in this study that allows to build the radionuclide directly into the DNA, namely 5-iododeoxyuridine. However, the lack of a satisfying vector to specifically target nuclear DNA of cancer cells remains a limitation since IUdR would also target healthy cells in S-phase. In addition, radiolabeled deoxyribonucleotides are known to have a rapid washout and the limitation to only target cells in the S-phase. However, it is well known that the percentage of cells in S-phase is higher in tumors compared to normal tissue [67]. In this *in vitro* study, lymphocytes were stimulated with PHA, since human lymphocytes reside predominantly in the G0 phase. In order to determine the fraction of cells that was in S-phase during the pulse labeling this cell proliferation was compared to non-stimulated lymphocytes of the same donor. As shown in **Figure 2**, incorporated ^{123}I radioactivity increased linearly with the added total activity and stimulated lymphocytes are able to incorporate approximately double the ^{123}IUdR amount than their non-stimulated counterparts. This trend was also noted by Kassis et al. in their studies using ^{125}IUdR [68]. A difference in S-phase fraction was observed between the different donors in this study. This variability is not unusual, since it is generally accepted that the time when PHA-stimulated lymphocytes enter their first S-phase can range from 24 h up to 100 h. Sörén et al. calculated that the total number of lymphocytes that entered S-phase during a 6 days culture period with PHA was approximately 40% of the initial population [69].

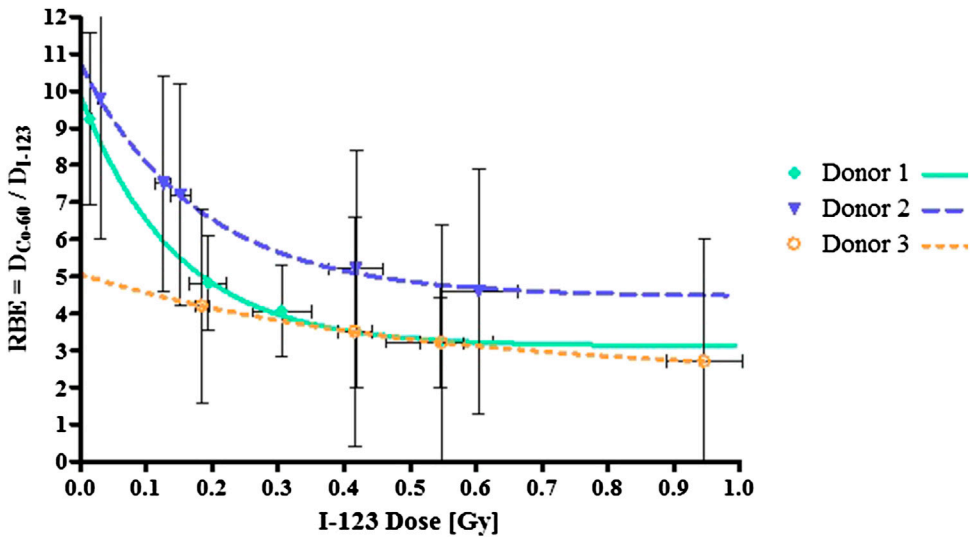

FIGURE 5 | RBE values based on the data points in the linear region of the ^{123}I dose-response curves for each donor. The error bars are the standard deviations of the mean RBE per dose point.

Previous cell killing experiments illustrated that DNA-incorporated ^{125}I is as effective as 5 MeV alpha-particles, which could be useful for the treatment of radioresistant tumors [19]. However, RBE values differ significantly between different studies. As previously mentioned, RBE values on ^{123}IUdR are limited, however some studies using ^{125}IUdR found RBE values that are within the range of RBE values observed in this study. Roa et al. reported RBE values of 7.9 ± 2.4 for ^{125}IUdR for spermatogonial cells [70]. The RBE relative to X-rays was estimated to be 7.3 by Kassis et al. in the ^{125}IUdR in the radiotherapy of brain tumors in rats [71]. While a study by Yasui *et al.* gives a RBE of 3.1 for ^{125}IUdR based on cell survival in Chinese hamster ovary cell line transfected with human estrogen receptor [72]. The difference in RBE values can be attributable to the fact that RBE is an empirical value which depends on several parameters such as radiation dose, biological effect and cells type, to only name a few. Another important consideration which is receiving growing attention recently, is the dose rate effect in targeted radionuclide therapy [73]. While the absorbed dose rate in conventional external beam radiotherapy is approximately 60 Gy/h, the irradiation in targeted radionuclide therapy is usually protracted from hours to days at a low dose rate of <1 Gy/h. This could be considered as a limitation in the current study, where the dose rates for the ^{123}IUdR exposures were very low (0.02 Gy/min at the activity level of 3.7 MBq) compared to the dose rate of the reference ^{60}Co γ-rays radiation quality (0.49 Gy/min) that was used to calculate the RBE. This limitation also applies to the previously mentioned studies where RBE values were calculated for Auger electron emitters. While it has long been considered that the dose rate dependence of high-LET radiation qualities is negligible, there is a growing body of evidence that suggest the contrary [73–76]. In addition, several studies describe an inverse dose rate effect, where increased cytotoxic effects per Gy are observed at low dose rates compared to high dose rates, while others studies contradict these findings [77–80]. Future studies are needed to confirm these observations and investigate the underlying mechanisms. Furthermore, the RBE values might also depend on the exposure conditions and the type of Auger emitter that was used. Direct comparison of various Auger electron emitting radionuclides is complicated due to the diverse electron emission spectra of these isotopes [67]. As already mentioned in the introduction, it was decided to use ^{123}I in this study instead of the more frequently used other Auger electron emitters, such as ^{125}I, in order to avoid the need to freeze the samples to accumulate disintegrations in the presence of anti-freeze agent DMSO. Since it is known that both the presence of DMSO and the irradiation of cells in frozen state has a radioprotective effect on cellular damage, it was decided that these conditions were best avoided for the assessment of the RBE of Auger electron emitters. This might also be important to have a clear idea of the impact of the two main damaging effects associated with Auger decay as described by Adelstein et al. [54]. Including a direct effect at the immediate decay site and an indirect effect many bases away from the decay site, which is due to radiolysis and the subsequent production of ROS. ^{123}I might also be more interesting for clinical applications than ^{125}I, due to its potential to function as a theranostic radionuclide. In addition, the physical half-life of radionuclides used in targeted radionuclide therapy should preferably be in the same order of magnitude as biological half-lives. It is therefore assumed that the most suitable physical half-life ranges from a few hours up to some days when a targeted approach is considered for disseminated cells [67].

The energy deposited in the cell is required to calculate the absorbed dose from the radioactive decay of ^{123}I. It has been shown that this depends highly on the subcellular localization of the Auger electron emitter [28, 44]. The nucleus of the target cell, its cytoplasm, and the extracellular region can be considered as source regions. In the study done by Fourie *et al.*, using Geant4 simulations, it was found that the energy deposited in the target nucleus per ^{123}I decay in the nucleus equals 4.1 keV/decay and the energy deposited in the nucleus per decay in the cytoplasm equals 0.5 keV/decay [44]. That is, the overall contribution from the cytoplasm source region to the energy deposited in the cell nucleus per decay is ~10% of the total. Furthermore, the contributions from decays external to the cell stemming from photons and the few high-energy conversion electrons amounts to a nuclear deposition of 0.024 keV/decay, less than 0.5% of the total energy deposited in the nucleus. Correspondingly, Makrigiorgos et al. concluded in their studies that cytoplasmic (7%) and external (<0.5%) dose contributions to the nucleus were negligible and that the cell survival mainly depends on the nuclear dose from ^{123}I decays in the cell nucleus [28]. However, Humm et al. stated that considerable *in vitro* experimental evidence exists to suggest that the absorbed dose to the nucleus alone is insufficient to predict the biological effects of Auger electron emitters concentrated in the cell nucleus [2]. Therefore, the microdosimetry calculations should include the energy deposition in all regions of the cell, especially when in use in comparison studies in radiobiological experiments. Using a calibrated microscopic image analysis system, the average cell diameter for our isolated and stimulated lymphocytes in suspension was found to be 9.8 ± 1.7 μm (~486 μm^3). The IAEA reports that peripheral lymphocytes 48 h after stimulation have a cell volume of about 500 μm^3 [81]. In our dosimetric calculations, a cellular diameter of 10 μm and a nuclear diameter of 8 μm were assumed. These mathematical assumptions were also used by Kassis *et al.* and Bousis et al. [24, 42, 47, 82]. The average energy deposited within the entire cell with the above geometry was calculated to be 4.5 keV per ^{123}I decay when distributed uniformly in the nucleus and this energy value was used to determine the absorbed dose values listed in **Table 1** [44].

There is a growing body of evidence that other sensitive sites besides the DNA, such as the cell membrane and mitochondria, could be critical targets in Auger emitter therapy. This would mean that nuclear uptake is not strictly required for Auger electron emitters in order exhibit their cytotoxic effect. The group of Pouget et al. could illustrate tumor growth delay with ^{125}I labeled non-internalizing antibodies [21, 27]. Furthermore, a different research group used an ^{111}In labeled non-internalizing

peptide F3, which induced a marked drop in colony survival and a delay in tumor growth [83]. However, the mechanisms by which membrane-associated Auger electron emitters can cause cytotoxicity has not yet been elucidated and should be the focus of future research efforts. In addition, recent studies also described radiation-induced bystander effects (RIBE) from Auger electron emitters, which might induce cytotoxicity in neighboring cells that have not been directly irradiated themselves [6]. These bystander effects might overcome the limitation that only a limited number of tumor cells get damaged by the Auger electrons directly because it is impossible to target every single cell in a tumor. These recent observations illustrate that nuclear localization might not be an absolute requirement and could open up the scope to label ^{123}I in the future with small molecules or peptides to develop novel targeted theranostic applications.

The current investigation found a linear increase in MNi induction with increasing ^{123}IUdR activity. This linear dose-response for ^{123}IUdR exposures is indicative of the high-LET nature of Auger electron emitters, which is also reflected in the high RBE that goes up to values of 10 for some of the donors. To our knowledge, no other study has evaluated chromosomal damage in human lymphocytes induced by DNA incorporated ^{123}I. Previous studies have reported a reduction in the variation of inter-donor radiosensitivity in lymphocytes for other forms of high-LET radiation like fast neutrons and α-particles when compared to low-LET radiation, however this could not be confirmed in this study. The current study provides useful information on the RBE of the Auger electron emitter ^{123}I, which might play a growing role as theranostic radionuclide in the near future.

DATA AVAILABILITY STATEMENT

The raw data supporting the conclusions of this article will be made available by the authors, without undue reservation.

ETHICS STATEMENT

The experiments were approved by the REC ethical clearance (reference number: S12/04/091) obtained from Stellenbosch University.

AUTHOR CONTRIBUTIONS

HF, SN. and JS. conceived and designed the experiments; XM performed lymphocyte isolations; SN, XM and HF. performed the radiobiology experiments under the guidance of PB; SN and DR performed the radiosynthesis and analysis, HF, SN, and CV analyzed the data; HF, SN and CV wrote the paper. RN, JS and JRZ are the grant holders in South Africa and secured funding for the experiments. All authors contributed to and approved the final version of the article, including the authorship list. The authors declare no conflict of interest.

ACKNOWLEDGMENTS

The authors would like to thank the Nuclear Technologies in Medicine and the Biosciences Initiative (NTeMBI), for their funding. NTeMBI is a national technology platform developed and managed by the South African Nuclear Energy Corporation (Necsa) and funded by the South African Department of Science and Innovation. The financial assistance of the National Research Foundation (NRF) toward this research is hereby acknowledged. Opinions expressed and conclusions arrived at, are those of the authors and are not necessarily to be attributed to the NRF. Additionally, this work was supported by a University Development Cooperation "VLIR Own Initiative Program" between Belgium and South Africa. The content of this manuscript has been published as part of the thesis of Hein Fourie [60].

REFERENCES

1. Howell RW. Auger processes in the 21st century. *Int J Radiat Biol* (2008) 84(12): 959–75. doi:10.1080/09553000802395527.
2. Humm JL, Howell RW, Rao DV. Dosimetry of auger-electron-emitting radionuclides: report no. 3 of AAPM nuclear medicine task group No. 6. *Med Phys* (1994) 21(12):1901–15. doi:10.1118/1.597227.
3. Auger P. The Auger effect. *Surf Sci* (1975) 48(1):1–8. doi:10.1016/0039-6028(75)90306-4.
4. Auger P. Sur les rayons β secondaires produits dans un gaz par des rayons X. *C R Acad Sci* (1923) 177:169–71.
5. Meitner L. Über die Entstehung der ?-Strahl-Spektren radioaktiver Substanzen. *Z Phys* (1922) 9(1):131–44. doi:10.1007/bf01326962.
6. Ku A, Facca VJ, Cai Z, Reilly RM. Auger electrons for cancer therapy–a review. *EJNMMI Radiopharmacy Chem* (2019) 4(1):27. doi:10.1186/s41181-019-0075-2.
7. Hofer KG, Hughes WL. Radiotoxicity of intranuclear tritium, 125 iodine and 131 iodine. *Radiat Res* (1971) 47(1):94–101. doi:10.2307/3573291.
8. Hofer KG, Harris CR, Smith JM. Radiotoxicity of Intracellular67Ga,125I and3H. *Int J Radiat Biol Relat Stud Phys Chem Med* (1975) 28(3):225–41. doi:10.1080/09553007514550991.
9. Martin RF, Feinendegen LE. The quest to exploit the Auger effect in cancer radiotherapy - a reflective review. *Int J Radiat Biol* (2016) 92(11):617–32. doi:10.3109/09553002.2015.1136854.
10. Buchegger F, Perillo-Adamer F, Dupertuis YM, Bischof Delaloye A. Auger radiation targeted into DNA: a therapy perspective. *Eur J Nucl Med Mol Imag* (2006) 33(11):1352–63. doi:10.1007/s00259-006-0187-2.
11. Salem R, Lewandowski RJ, Atassi B, Gordon SC, Gates VL, Barakat O, et al. Treatment of unresectable hepatocellular carcinoma with use of 90Y microspheres (TheraSphere): safety, tumor response, and survival. *J Vasc Intervent Radiol* (2005) 16(12):1627–39. doi:10.1097/01.rvi.0000184594.01661.81.
12. Vallabhajosula S, Goldsmith SJ, Hamacher KA, Kostakoglu L, Konishi S, Milowski MI, et al. Prediction of myelotoxicity based on bone marrow radiation-absorbed dose: radioimmunotherapy studies using 90Y- and 177Lu-labeled J591 antibodies specific for prostate-specific membrane antigen. *J Nucl Med* (2005) 46(5):850–8.
13. Kozempel J, Mokhodoeva O, Vlk M. Progress in targeted alpha-particle therapy. What we learned about recoils release from in vivo generators. *Molecules* (2018) 23(3):581. doi:10.3390/molecules23030581.
14. Tafreshi NK, Doligalski ML, Tichacek CJ, Pandya DN, Budzevich MM, El-Haddad G, et al. Development of targeted alpha particle therapy for solid tumors. *Molecules* (2019) 24(23):4314. doi:10.3390/molecules24234314.

15. Kassis AI. Molecular and cellular radiobiological effects of Auger emitting radionuclides. *Radiat Protect Dosim* (2011) 143(2–4):241–7. doi:10.1093/rpd/ncq385.
16. Kassis AI, Adelstein SJ. Radiobiologic principles in radionuclide therapy. *J Nucl Med* (2005) 46 (Suppl. 1):4s–12s.
17. Haberkorn U, Giesel F, Morgenstern A, Kratochwil C. The future of radioligand therapy: α, β, or both? *J Nucl Med* (2017) 58(7):1017–8. doi:10.2967/jnumed.117.190124.
18. Poty S, Francesconi LC, McDevitt MR, Morris MJ, Lewis JS. α-Emitters for radiotherapy: from basic Radiochemistry to clinical studies-Part 1. *J Nucl Med* (2018) 59(6):878–84. doi:10.2967/jnumed.116.186338.
19. Rao D, Howell R, Narra V, Govelitz G, Sastry KR. *In-vivo* radiotoxicity of DNA-incorporated 125I compared with that of densely ionising alpha-particles. *Lancet* (1989) 334(8664):650–3. doi:10.1016/s0140-6736(89)90896-9.
20. Paillas S, Ladjohounlou R, Lozza C, Pichard A, Boudousq V, Jarlier M, et al. Localized irradiation of cell membrane by auger electrons is cytotoxic through oxidative stress-mediated nontargeted effects. *Antioxidants Redox Signal* (2016) 25(8):467–84. doi:10.1089/ars.2015.6309.
21. Pouget J-P, Santoro L, Raymond L, Chouin N, Bardiès M, Bascoul-Mollevi C, et al. Cell membrane is a more sensitive target than cytoplasm to dense ionization produced by auger electrons. *Radiat Res* (2008) 170(2):192–200. doi:10.1667/rr1359.1.
22. Chastel A, Worm DJ, Alves ID, Vimont D, Petrel M, Fernandez S, et al. Design, synthesis, and biological evaluation of a multifunctional neuropeptide-Y conjugate for selective nuclear delivery of radiolanthanides. *EJNMMI Res* (2020) 10(1):16. doi:10.1186/s13550-020-0612-8.
23. Goddu SM, Narra VR, Harapanhalli RS, Howell RW, Rao DV. Radioprotection by dmso against the biological effects of incorporated radionuclides *in Vivo*: comparison with other radioprotectors and evidence for indirect action of auger electrons. *Acta Oncol* (1996) 35(7):901–7. doi:10.3109/02841869609104044.
24. Kassis AI, Fayad F, Kinsey BM, Sastry KSR, Taube RA, Adelstein SJ. Radiotoxicity of 125 I in mammalian cells. *Radiat Res* (1987) 111(2):305–18. doi:10.2307/3576987.
25. Mothersill C, Rusin A, Fernandez-Palomo C, Seymour C. History of bystander effects research 1905-present; what is in a name? *Int J Radiat Biol* (2018) 94(8):696–707. doi:10.1080/09553002.2017.1398436.
26. Boyd M, Ross SC, Dorrens J, Fullerton NE, Tan KW, Zalutsky MR, et al. Radiation-induced biologic bystander effect elicited *in vitro* by targeted radiopharmaceuticals labeled with alpha-, beta-, and auger electron-emitting radionuclides. *J Nucl Med* (2006) 47(6):1007–15.
27. Paillas S, Ladjohounlou R, Lozza C, Pichard A, Boudousq V, Jarlier M, et al. Localized irradiation of cell membrane by auger electrons is cytotoxic through oxidative stress-mediated nontargeted effects. *Antioxidants Redox Signal* (2016) 25(8):467–84. doi:10.1089/ars.2015.6309.
28. Makrigiorgos GM, Kassis AI, Baranowska-Kortylewicz J, McElvany KD, Welch MJ, Sastry KSR, et al. Radiotoxicity of 5-[123 I]iodo-2'-deoxyuridine in V79 cells: a comparison with 5-[125 I]iodo-2'-deoxyuridine. *Radiat Res* (1989) 118(3):532–44. doi:10.2307/3577411.
29. Sedelnikova OA, Rogakou EP, Panyutin IG, Bonner WM. Quantitative detection of (125)IdU-induced DNA double-strand breaks with gamma-H2AX antibody. *Radiat Res* (2002) 158(4):486–92. doi:10.1667/0033-7587(2002)158[0486:qdoiid]2.0.co;2.
30. Piron B, Paillas S, Boudousq V, Pelegrin A, Bascoul-Mollevi C, Chouin N, et al. DNA damage-centered signaling pathways are effectively activated during low dose-rate Auger radioimmunotherapy. *Nucl Med Biol* (2014) 41(Suppl. 1):e75–83. doi:10.1016/j.nucmedbio.2014.01.012
31. Woo DV, Li D, Mattis JA, Steplewski Z. Selective chromosomal damage and cytotoxicity of 125I-labeled monoclonal antibody 17-1a in human cancer cells. *Cancer Res* (1989) 49(11):2952–8.
32. Schmitz S, Oskamp D, Pomplun E, Kriehuber R. Chromosome aberrations induced by the Auger electron emitter 125I. *Mutat Res Genet Toxicol Environ Mutagen* (2015) 793:64–70. doi:10.1016/j.mrgentox.2015.08.007.
33. Schwartz JL, Mustafi R, Hughes A, DeSombre ER. DNA and chromosome breaks induced by iodine- 123-labeled estrogen in Chinese hamster ovary cells. *Radiat Res* (1996) 146(2):151–8. doi:10.2307/3579587.
34. Hindorf C, Emfietzoglou D, Lindén O, Kostarelos K, Strand S-E. Internal microdosimetry for single cells in radioimmunotherapy of B-cell lymphoma. *Canc Biother Rad* (2005) 20(2):224–30. doi:10.1089/cbr.2005.20.224.
35. Hindorf C, Emfietzoglou D, Lindén O, Bousis C, Fotopoulos A, Kostarelos K, et al. Single-cell dosimetry for radioimmunotherapy of B-cell lymphoma patients with special reference to leukemic spread. *Canc Biother Rad* (2007) 22(3):357–66. doi:10.1089/cbr.2007.347.
36. Fenech M. Cytokinesis-block micronucleus cytome assay. *Nat Protoc* (2007) 2(5):1084–104. doi:10.1038/nprot.2007.77.
37. Vral A, Fenech M, Thierens H. The micronucleus assay as a biological dosimeter of *in vivo* ionising radiation exposure. *Mutagenesis* (2011) 26:11–7. doi:10.1093/mutage/geq078.
38. Howell RW, Rao DV, Sastry KSR. Macroscopic dosimetry for radioimmunotherapy: nonuniform activity distributions in solid tumors. *Med Phys* (1989) 16:66–74. doi:10.1118/1.596404.
39. Goddu SM, Howell RW, Rao DV. Cellular dosimetry: absorbed fractions for monoenergetic electron and alpha particle sources and S-values for radionuclides uniformly distributed in different cell compartments. *J Nucl Med* (1994) 35:303–16.
40. Nikjoo N, Emfietzoglou D, Charlton DE. The Auger effect in physical and biological research. *Int J Radiat Biol* (2008) 84(12):1001–26. doi:10.1080/09553000802460172.
41. Bousis C, Emfietzoglou D, Nikjoo H. Calculations of absorbed fractions in small water spheres for low-energy monoenergetic electrons and the Auger-emitting radionuclides123I and125I. *Int J Radiat Biol* (2012) 88(12):916–21. doi:10.3109/09553002.2012.666003.
42. Bousis C, Emfietzoglou D, Hadjidoukas P, Nikjoo H. Monte Carlo single-cell dosimetry of Auger-electron emitting radionuclides. *Phys Med Biol* (2010) 55(9):2555–72. doi:10.1088/0031-9155/55/9/009.
43. Incerti S, Douglass M, Penfold S, Guatelli S, Bezak E. Review of Geant4-DNA applications for micro and nanoscale simulations. *Phys Med* (2016) 32:1187–200. doi:10.1016/j.ejmp.2016.09.007.
44. Fourie H, Newman RT, Slabbert JP. Microdosimetry of the Auger electron emitting123I radionuclide using Geant4-DNA simulations. *Phys Med Biol* (2015) 60(8):3333–46. doi:10.1088/0031-9155/60/8/3333.
45. Uddin MJ, Crews BC, Blobaum AL, Kingsley PJ, Ghebreselasie K, Saleh SS, et al. Synthesis and evaluation of [123I]-indomethacin derivatives as COX-2 targeted imaging agents. *J Label Compd Radiopharm* (2009) 52(9):387–93. doi:10.1002/jlcr.1615.
46. Cecchini MJ, Amiri M, Dick FA. Analysis of cell cycle position in mammalian cells. *J Vis Exp* (2012) (59):3491. doi:10.3791/3491.
47. Kassis AI, Makrigiorgos GM, Adelstein SJ. Implications of radiobiological and dosimetric studies of DNA-incorporated 123I: the use of the auger effect as a biological probe at the nanometre level. *Radiat Protect Dosim* (1990) 31(1–4):333–8. doi:10.1093/rpd/31.1-4.333.
48. Šefl M, Kyriakou I, Emfietzoglou D. Technical Note: impact of cell repopulation and radionuclide uptake phase on cell survival. *Med Phys* (2016) 43(6):2715–20. doi:10.1118/1.4948504
49. Fourie H, Newman RT, Slabbert JP. Microdosimetry of the Auger electron emitting123I radionuclide using Geant4-DNA simulations. *Phys Med Biol* (2015) 60:3333–46. doi:10.1088/0031-9155/60/8/3333.
50. Šefl M, Incerti S, Papamichael G, Emfietzoglou D. Calculation of cellular S-values using Geant4-DNA: the effect of cell geometry. *Appl Radiat Isot* (2015) 104:113–23. doi:10.1016/j.apradiso.2015.06.027.
51. Dale RG, Jones B. The assessment of RBE effects using the concept of biologically effective dose. *Int J Radiat Oncol Biol Phys* (1999) 43(3):639–45. doi:10.1016/s0360-3016(98)00364-2.
52. Carabe-Fernandez A, Dale RG, Jones B. The incorporation of the concept of minimum RBE (RbEmin) into the linear-quadratic model and the potential for improved radiobiological analysis of high-LET treatments. *Int J Radiat Biol* (2007) 83(1):27–39. doi:10.1080/09553000601087176.
53. Clayden J, Greeves N, Warren S, Wothers P. *Organic chemistry*. New York, NY: Oxford University Press (2001) 1133 p.
54. Adelstein SJ, Kassis AI, Bodei L, Mariani G. Radiotoxicity of iodine-125 and other auger-electron-emitting radionuclides: background to therapy. *Canc Biother Rad* (2003) 18(3):301–16. doi:10.1089/108497803322285062.

55. Rosenkranz AA, Slastnikova TA, Durymanov MO, Georgiev GP, Sobolev AS. Exploiting active nuclear import for efficient delivery of Auger electron emitters into the cell nucleus. *Int J Radiat Biol* (2020). 1–11. doi:10.1080/09553002.2020.1815889.
56. Pirovano G, Jannetti SA, Carter LM, Sadique A, Kossatz S, Guru N, et al. Targeted brain tumor radiotherapy using an auger emitter. *Clin Cancer Res* (2020) 26(12):2871–81. doi:10.1158/1078-0432.CCR-19-2440
57. Shen CJ, Minn I, Hobbs RF, Chen Y, Josefsson A, Brummet M, et al. Auger radiopharmaceutical therapy targeting prostate-specific membrane antigen in a micrometastatic model of prostate cancer. *Theranostics* (2020) 10(7):2888–96. doi:10.7150/thno.38882.
58. McLean JR, Blakey DH, Douglas GR, Bayley J. The Auger electron dosimetry of indium-111 in mammalian cells *in vitro*. *Radiat Res* (1989) 119(2):205–18. doi:10.2307/3577614.
59. Sundellbergman S, Bergman R, Johanson K. Chromosome damage induced by decay of 3H and 125I incorporated into DNA of Chinese hamster cells. *Mutat Res Fund Mol Mech Mutagen* (1985) 149(2):257–63. doi:10.1016/0027-5107(85)90032-6.
60. Bingham D, Bonner PT, Cox R, Edwards AA, Gardin I, Haines JW, et al. Comparison of cytogenetic damage in cultured cells from cobalt-60 gamma-radiation and the Auger emitter zinc-65. *Int J Radiat Biol* (2000) 76(9):1223–31. doi:10.1080/09553000050134456.
61. Slabbert JP, August L, Vral A, Symons J. The relative biological effectiveness of a high energy neutron beam for micronuclei induction in T-lymphocytes of different individuals. *Radiat Meas* (2010) 45(10):1455–7. doi:10.1016/j.radmeas.2010.06.060.
62. Norppa H, Falck GC. What do human micronuclei contain? *Mutagenesis* (2003) 18(3):221–33. doi:10.1093/mutage/18.3.221.
63. Vral A, Verhaegen F, Thierens H, De Ridder L. Micronuclei induced by fast neutrons Versus60Co γ-rays in human peripheral blood lymphocytes. *Int J Radiat Biol* (1994) 65(3):321–8. doi:10.1080/09553009414550381.
64. Bavelaar BM, Lee BQ, Gill MR, Falzone N, Vallis KA. Subcellular targeting of theranostic radionuclides. *Front Pharmacol* (2018) 9:996. doi:10.3389/fphar.2018.00996.
65. Kassis AI. Cancer therapy with Auger electrons: are we almost there? *J Nucl Med* (2003) 44(9):1479–81.
66. Capello A, Krenning E, Bernard B, Reubi J-C, Breeman W, de Jong M. 111In-labelled somatostatin analogues in a rat tumour model: somatostatin receptor status and effects of peptide receptor radionuclide therapy. *Eur J Nucl Med Mol Imag* (2005) 32(11):1288–95. doi:10.1007/s00259-005-1877-x.
67. Cornelissen B, A Vallis K. Targeting the nucleus: an overview of Auger-electron radionuclide therapy. *Cddt* (2010) 7(4):263–79. doi:10.2174/157016310793360657.
68. Kassis AI, Sastry KSR, Adelstein SJ. Kinetics of uptake, retention, and radiotoxicity of 125 IUdR in mammalian cells: implications of localized energy deposition by auger processes. *Radiat Res* (1987) 109(1):78–89. doi:10.2307/3576869.
69. Sörén L. Variability of the time at which PHA-stimulated lymphocytes initiate DNA synthesis. *Exp Cell Res* (1973) 78(1):201–8. doi:10.1016/0014-4827(73)90055-4.
70. Rao DV, Narra VR, Howell RW, Lanka VK, Sastry KSR. Induction of sperm head abnormalities by incorporated radionuclides: dependence on subcellular distribution, type of radiation, dose rate, and presence of radioprotectors. *Radiat Res* (1991) 125(1):89–97. doi:10.2307/3577986.
71. Kassis AI, Wen PY, Van den Abbeele AD, Baranowska-Kortylewicz J, Makrigiorgos GM, Metz KR, et al. 5–[125I]iodo-2'-deoxyuridine in the radiotherapy of brain tumors in rats. *J Nucl Med* (1998) 39(7):1148–54.
72. Yasui LS, Hughes A, DeSombre ER. Production of clustered DNA damage by125I decay. *Acta Oncol* (2000) 39(6):739–40. doi:10.1080/028418600750063811.
73. Pouget J-P, Lozza C, Deshayes E, Boudousq V, Navarro-Teulon I. Introduction to radiobiology of targeted radionuclide therapy. *Front Med* (2015) 2:12. doi:10.3389/fmed.2015.00012.
74. Stevens DL, Bradley S, Goodhead DT, Hill MA. The influence of dose rate on the induction of chromosome aberrations and gene mutation after exposure of plateau phase V79–4 cells with high-LET alpha particles. *Radiat Res* (2014) 182(3):331–7. doi:10.1667/rr13746.1.
75. Nair S, Engelbrecht M, Miles X, Ndimba R, Fisher R, du Plessis P, et al. The impact of dose rate on DNA double-strand break formation and repair in human lymphocytes exposed to fast neutron irradiation. *Int J Mol Sci* (2019) 20(21):5350. doi:10.3390/ijms20215350.
76. Sgouros G, Knox SJ, Joiner MC, Morgan WF, Kassis AI. MIRD continuing education: bystander and low dose-rate effects: are these relevant to radionuclide therapy? *J Nucl Med* (2007) 48(10):1683–91. doi:10.2967/jnumed.105.028183.
77. Matsuya Y, McMahon SJ, Tsutsumi K, Sasaki K, Okuyama G, Yoshii Y, et al. Investigation of dose-rate effects and cell-cycle distribution under protracted exposure to ionizing radiation for various dose-rates. *Sci Rep* (2018) 8(1):8287. doi:10.1038/s41598-018-26556-5.
78. Barnard SGR, McCarron R, Moquet J, Quinlan R, Ainsbury E. Inverse dose-rate effect of ionising radiation on residual 53BP1 foci in the eye lens. *Sci Rep* (2019) 9(1):10418. doi:10.1038/s41598-019-46893-3.
79. Mitchell JB, Bedford JS, Bailey SM. Dose-rate effects in mammalian cells in culture: III. Comparison of cell killing and cell proliferation during continuous irradiation for six different cell lines. *Radiat Res* (1979) 79(3):537–51. doi:10.2307/3575179.
80. Gholami YH, Willowson KP, Forwood NJ, Harvie R, Hardcastle N, Bromley R, et al. Comparison of radiobiological parameters for (90)Y radionuclide therapy (RNT) and external beam radiotherapy (EBRT) *in vitro*. *EJNMMI phys* (2018) 5(1):18. doi:10.1186/s40658-018-0217-8.
81. IAEA-EPR. *Cytogenetic dosimetry: application in preparedness for and response to radiation emergencies*. Vienna, Austria 2011.
82. Emfietzoglou D, Bousis C, Hindorf C, Fotopoulos A, Pathak A, Kostarelos K. A Monte Carlo study of energy deposition at the sub-cellular level for application to targeted radionuclide therapy with low–energy electron emitters. *Nucl Instrum Methods Phys Res Sect B Atoms* (2007) 256(1):547–53. doi:10.1016/j.nimb.2006.12.055.
83. Drecoll E, Gaertner FC, Miederer M, Blechert B, Vallon M, Müller JM, et al. Treatment of peritoneal carcinomatosis by targeted delivery of the radio-labeled tumor homing peptide bi-DTPA-[F3]2 into the nucleus of tumor cells. *PloS One* (2009) 4(5):e5715. doi:10.1371/journal.pone.0005715.

Conflict of Interest: Author Prof. JRZ is employed by The South African Nuclear Energy Corporation.

The remaining authors declare that the research was conducted in the absence of any commercial or financial relationships that could be construed as a potential conflict of interest.